Chapter 4

Single-Pulse Studies at 35 MHz : Fluctuation Spectra

In section 1.2, we described the phenomena observed at single-pulse time scales (typically a few milliseconds to a few tens of seconds). Earlier we also elaborated Rankin's scheme of pulsar classification from their average properties. Core and conal components show qualitatively different types of fluctuation behavior. We now consider the conventional tools to study the various types of phenomena. These tools include the fluctuation spectra of pulsars, correlation analysis, and studies of modulation indices etc. Fluctuation power spectral features are considered to be among the stable and distinguishing characteristics of pulsars just as the profile shapes, polarization, etc. They have been studied in detail at meter wavelengths for most of the bright sources. In this chapter, we describe these techniques along with the relevant terminology, and also discuss some of the other techniques used to study single-pulse sequences. We present some results obtained by applying these techniques to our 35-MHz data on a few bright pulsars observed using GEETEE.

4.1 Data sets

We studied eight bright pulsars in our observed sample for their single-pulse properties. Some details of the chosen pulsars, such as their Rankin classification, fluctuation properties observed at meter wavelengths, and details of our data sets are listed in the table below.

4.2 Fluctuation spectra

A very powerful and conventional tool to study single-pulse phenomena is the spectral analysis of fluctuations in intensity at separate longitudes. The fluctuation spectra bring out any systematic of singlepulse fluctuations as a function of time (pulse number) and pulse longitude much more clearly than possible in the time domain.

Pulsar Name	Rankin Classification	Fluctuation features reported at meter wavelengths c/P_1	Single-pulse phenomena observed at meter wavelengths[1]	Number of data sets studied at 34.5 MHz
B0320+39	T	0.118	D[2]	1
B0628-28	S_d	none	D[3]	1
B0834+06	D	0.463	N[4], O[5]	5
B0943+10	S_d	0.46	D[6], M, O[7]	6
B0950+08	D	0.46	none!	4
B1133+16	D	0.19	M[8], O[9]	1
B1919+21	nD	0.233	D[6], N[4]	1
B2016+28	S_d	0.0667-0.111	D[6]	1

Table 4.1: [1] $D \equiv$ drifting, N≡nulling, M≡ Profile Modes, O≡OPM.
References: (2) Izvekova, Kuzmin & Shitov, 1982. (3) Ashworth, 1982, reports a sporadic drift, no reported P_3 at meter wavelengths. (4) Ritchings, 1976. (5) Gil, 1987. (6) Taylor & Huguenin, 1971 (7) Suleymanova et *al.*, 1998. (8) Nowakowski, 1996, reports a new phenomenon in this pulsar. (9) Stinebring et *al.*, 1984

4.2.1 Longitude-resolved fluctuation spectra

A 2-D matrix, $I_{jk} \equiv I(\varphi_j, n)$, of intensity as a function of longitude, φ, and pulse number, n, is created from a pulsar time series, where the longitude $\varphi(-180° \leq 9 \leq 180°)$ is usually defined with respect to some fiducial point on the pulse. Such a spectral analysis is usually confined to a narrow window around the pulse region (typically of width 40° in our case). A 1-D data array in time (pulse number) from a fixed longitude φ_j is extracted from the array I_{jk}, and is Fourier analyzed to obtain Fourier spectra, $P(\lambda_j, f,)$, in the standard way, where f_m denotes the fluctuation frequency. This analysis is repeated for all the longitudes of interest.

Such spectra are usually represented in 2-D plots of φ_j *vs.* f,, with P represented in color, or contour levels. Represented in this form, such a spectrum is referred to as a longitude-resolved fluctuation spectrum, or lrf-spectrum in short. An example of such an unnormaliied spectrum is presented in the figure 4.1.

Some explanation regarding the figure layout is in order. We have plotted, in the left panel, the average profile of the pulsar. Fluctuation spectra for each of the longitudes were computed, as explained above. The individual spectra at each longitude are plotted against the fluctuation frequency, measured in cycles per period (denoted by c/P_1), in the central panel. The bottom panel displays the combined spectrum after adding contributions from all the longitudes in each frequency bin.

While dealing with the lrf-spectra it is important to be aware of the following issues:

- Since a given longitude is sampled only once during the pulsar rotation cycle, the maximum frequency in the spectrum is 0.5 cycles/period. A higher frequency modulation (faster than $0.5\,c/P_1$) will get aliased at a lower frequency in our spectrum and this is true of any fluctuation feature in the spectrum.

- The statistical error in the determination of the frequency of any fluctuation feature depends on the spectral resolution and signal-to-noise of the feature. The resolution in the spectrum is given by $Af = \frac{1}{N} c/P_1$, where N is the total number of pulses used in the computation of the spectrum ($\Delta f \sim 8 \times 10^{-3}\, c/P_1$ for a 128 pulse transform). For the present study, we used typically 128 or 256 pulses.

- The sharpness parameter, *i.e.* the Q-value, of a feature present at a frequency f and of width 6f , defined as $f/\delta f$, is determined by the spectral resolution and by the stability of the frequency of the associated modulation aver the duration of the pulse sequence used.

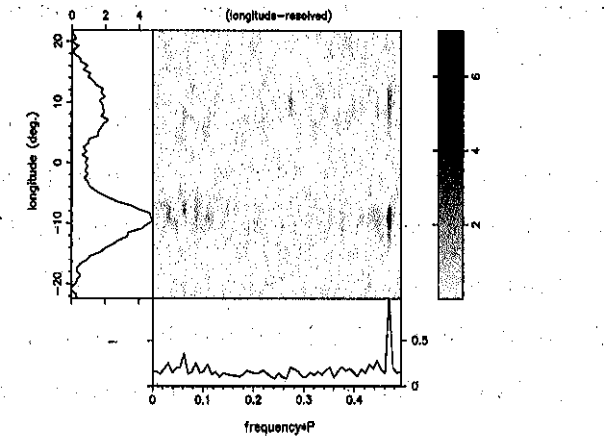

Figure 4.1: An lrf-spectrum of B0943+10, derived using a 128-pulse transform. The spectra appear in grey-scale corresponding to longitudes in the average profile plotted on the left. The combined spectrum from all longitudes is shown in the bottom panel

We now concentrate on figure 4.1 (lrf-spectrum). The lrf-spectrum of B0943+10 exhibits some typical attributes of fluctuation spectra of a pulsar. Most observed spectra at meter wavelengths consist of the following three distinct components :

- A red noise component which increases in strength with decreasing fluctuation frequency. It is attributed to interstellar scintillation, slow modulation intrinsic to the pulsar emission, and/or possible slow variations in the instrumental gain. The contribution due to scintillation varies for different pulsars, and also depends on the observing frequency and bandwidth. Given that our 1-MHz bandwidth $\gg$ decorrelation bandwidth, we do not expect scintillations to affect our spectra. Mostly in our spectra, the red component contribution falls in the first bin of the spectrum closest to the zero frequency.

- A white component resulting from erratic pulse-to-pulse variations. This belongs to random fluctuations, either intrinsic or due to propagation effects, in the non-fluctuating component of the pulsar emission. This forms a baseline (or pedestal) in the spectra, over and above which apparent distinct features, if any, may be, seen.

- One or more distinct features, and their occasional harmonics, due to systematic fluctuation phenomena, such as subpulse drifting, or profile amplitude modulation. The amplitudes of such fluctuations vary from pulsar to pulsar, and can be as large as 100% in some cases.

The feature at $0.469\,c/P_1$, in figure 4.1, represents the drifting part of pulsed emission from the pulsar. The feature is present in the region of the pulse, and displays a Q-value of more than 128, the length of the transform in this case. Some excess power is also evident at $0.06\,c/P_1$,

over and above the white noise contribution present in the spectrum. The red noise contribution to this spectrum is negligible.

The lrf-spectrum gives us a wealth of information about the fluctuations present in the sequence, but also has a serious drawback of aliasing due to poor sampling of a fluctuation in each longitude only once in a pulse period; *e.g.* it can happen, that the strong feature (in the figure 4.1) actually corresponds to a much higher frequency and is aliased to its current position in the spectrum. The effect of aliasing also hinders determination of any possible harmonic relationship between various features. As we will discuss in particular cases in the next chapter, this problem has been a big obstacle in understanding the origin of such fluctuations.

4.2.2 Raw spectrum and the issue of aliasing

To resolve the issue of aliasing in lrf-spectra, we need to overcome the basic limitation of sampling. But, the fluctuations are sampled more than once in the finite duration of the pulse. We can, therefore, combine the fluctuation spectra in different longitude bins with appropriate phases corresponding to the longitude separation. This approach has been advanced by Deshpande & Rankin, 1999 (DRa), and Deshpande & Rankin, 2001 (paper-I) in the manner described below (see also Deshpande, 2000).

In practice, we achieve the above by simply Fourier transforming the entire continuous sequence, which can be reconstructed (from the "gated" version) by using the available samples on pulse, and filling the rest of the longitude region with zeros. Such (power) spectra can be computed for suitable blocks of 256 or 512 pulses and then averaged. In this process, the pulse sequence is effectively multiplied by a periodic "window" function. It leads to convolution of the raw pulse sequence with the Fourier spectrum of the window function used. Hence, it is necessary that the entire pulse window is sampled in the gating process, and that the "baseline" in the off-pulse region is flat, since the spectral features corresponding to the pulsar signal can be otherwise distorted. The windowing function then only smooths the noise without distorting the pulsar spectrum, and hence enhances the signal-to-noise ratio of the spectral features of interest.

If there were a single-tone sinusoidal wave (of period, say P_2, which is not, in general, an integral submultiple of P_1) plus a dc level (greater than the tone amplitude) modulating a steady pulsed emission (say of a "single" Gaussian profile), the Fourier spectrum of the resultant time series would be a convolution of the spectrum of the average-pulse profile (a set of harmonics in the frequency domain with a Gaussian envelope) and the delta function corresponding to the dc and the sine wave. This situation is elaborated in figure 4.2, where the period of the modulation, say, P_2,

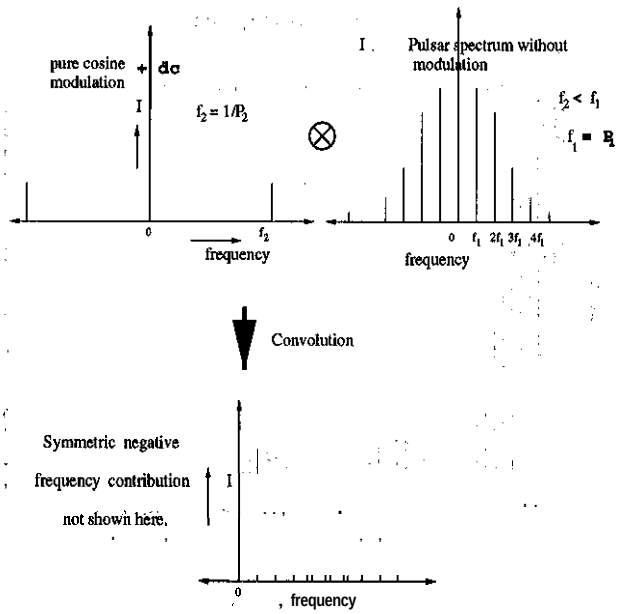

Figure 4.2: Effect ,of a sinusoidal modulation as seen in the pulsar spectrum.

is much shorter than the pulse period, P_1. If the average-pulse profile was more complex and the modulation frequency $(1/P_2)$ was much higher than pulsar frequency, then the resultant spectrum would display a complex envelope of harmonic peaks of the mean pulse profile convoluted with the 6-functions. This simplified model captures the main features of the raw fluctuation spectra we would encounter in the case of additional periodic phase or amplitude modulation of the pulsar signals.

The result of such a computation of the raw fluctuation spectrum in the case of B0943+10 is given in figure 4.3, where only the positive half of the symmetric spectrum is plotted as a function of frequency (counted in the units of pulsar rotation frequency $1/P_1$). We now try to understand the information present in this plot. Note, the amplitude of the frequency components at integral multiples of $1/P_1$. These are the Fourier components of the "average" profile of the pulsar, which consist of contributions from its "base" profile–or the steady component of the emission–as well as from the fluctuating part seen on an average. The harmonics decline by the harmonic number 10, and rise again at harmonic number of 16, again decay to half the value at about harmonic number 20. The second peak in the harmonic strengths at harmonic number of 16 corresponds to the longitude separation of the two components' peaks in the average pulse profile (about 20°). Now, notice the spectral components at about half integral frequencies (actually, N + 0.541 c/P_1). The peaks of these components are modulated by a two-peaked function, with one of the peaks falling close to the 16^{th} harmonic and the other close to the 32^{nd}. It is convenient to interpret this in the framework

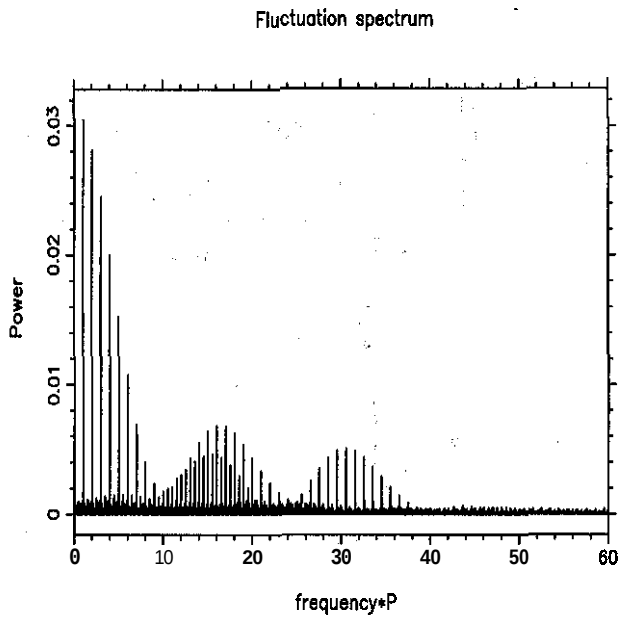

Figure **4.3:** Raw hrf-spectrum of B0943+10 data set.

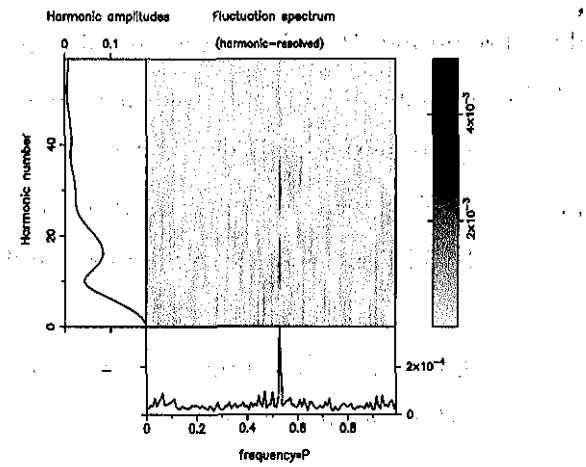

Figure **4.4:** Hrf-spectrum of B0943+10 data set.

of the above model, as a result of the convolution of frequency components of the average profile with the &function of a sinusoidal modulation. The frequency of the modulation would then be **15.541** c/P_1. However, in this case, a direct interpretation in terms of P_2 as a subpulse spacing also would be erroneous due to possibly somewhat central viewing. The double Gaussian-like shape of the peaks of the modulation harmonics define the shape of the "envelope" followed by the subpulses as they drift in longitude. And, the fact that no higher harmonic of the primary modulation is detectable in the spectrum shows, that the subpulse widths are nearly equal to their separations.

Jwt to make things clearer, we present the fluctuation spectrum in figure **4.3** in a different manner following Deshpande & Rankin, **2001** (paper-I), where we stack the successive sections in

the spectrum of width $(1/P_1)$ one above another as shown in figure 4.4. We see immediately that the principal modulation feature now falls at a frequency of about $0.541\,c/P_1$. The power at a frequency of $1/P_1$ and its harmonics–which comprise the "average" profile of the pulsar–are shown in the left-hand panel. The fluctuation at other frequencies, as a function of $1/P_1$ interval, is shown in the body of the figure; and the integral of this fluctuation power, summed into a single $1/P_1$ band, is displayed in the bottom panel. We refer to this spectral representation as an "harmonic-resolved fluctuation spectrum" (hereafter "HRF-spectrum").

An hrf-spectrum can also distinguish between the two types of pulse modulations encountered, viz. amplitude- and phase-modulations. Let us understand this in terms of the figure 4.2, which represents the case of a phase modulation (subpulse drift), when $\frac{1}{P_2} \gg \frac{1}{P_1}$. If we fold the spectrum in the manner of hrf-spectra and integrate only the positive side of the spectrum, the harmonics that dominate are at $(N + 1/P_3)$, which contribute to the spectrum in the bottom panel of hrf-spectra. The contribution due to the set of harmonics around $-f_2$ $(\equiv -1/P_2)$ will be negligible. Thus, the bottom panel will contain one strong peak corresponding to the actual frequency of the modulation. In case the period of the modulation is longer than the pulse period (*i.e.* $P_2 \gtrsim P_1$), it is called an amplitude modulation. Such a spectrum will show a pair of near symmetric features around $0.5\ c/P_1$ in the bottom panel. The case of B0943+10, presented in figure 4.4, clearly shows that the modulation is related to subpulse drifting, whereas figure 4.6 displays the spectrum in the case of B0834+06, a pulsar displaying a strong amplitude modulation in the pulse sequence.

Figure 4.3 presents exactly the same information as in figure 4.4, but in a slightly more direct way. No information is suppressed here, the two figures display the amplitude of all Fourier components of the pulse sequence. For further discussion, we will concentrate on both the lrf- & hrf-spectra.

So far we detailed our spectral analysis methods of studying fluctuations, and now we discuss the lrf-spectra of a set of pulsars in some detail.

B0943+10

This pulsar is known to be a steady "drifter", classified in profile types as a conal single (S_d) by Rankin (1993) based on meter wavelength data. However, the 34.5-MHz profile is a clearly resolved double ('D') profile. The pulsar data show a sharp peak in the lrf-spectrum, as shown in the figures 4.5 (a, b) close to $0.5\,c/P_1$. This feature is associated with the observed subpulse drift at meter wavelengths. This phase-modulation feature in figure 4.5(a) has a Q-value of ≥ 200. The frequency of the phase modulation was seen to vary by about 2% over different data sets. Such a

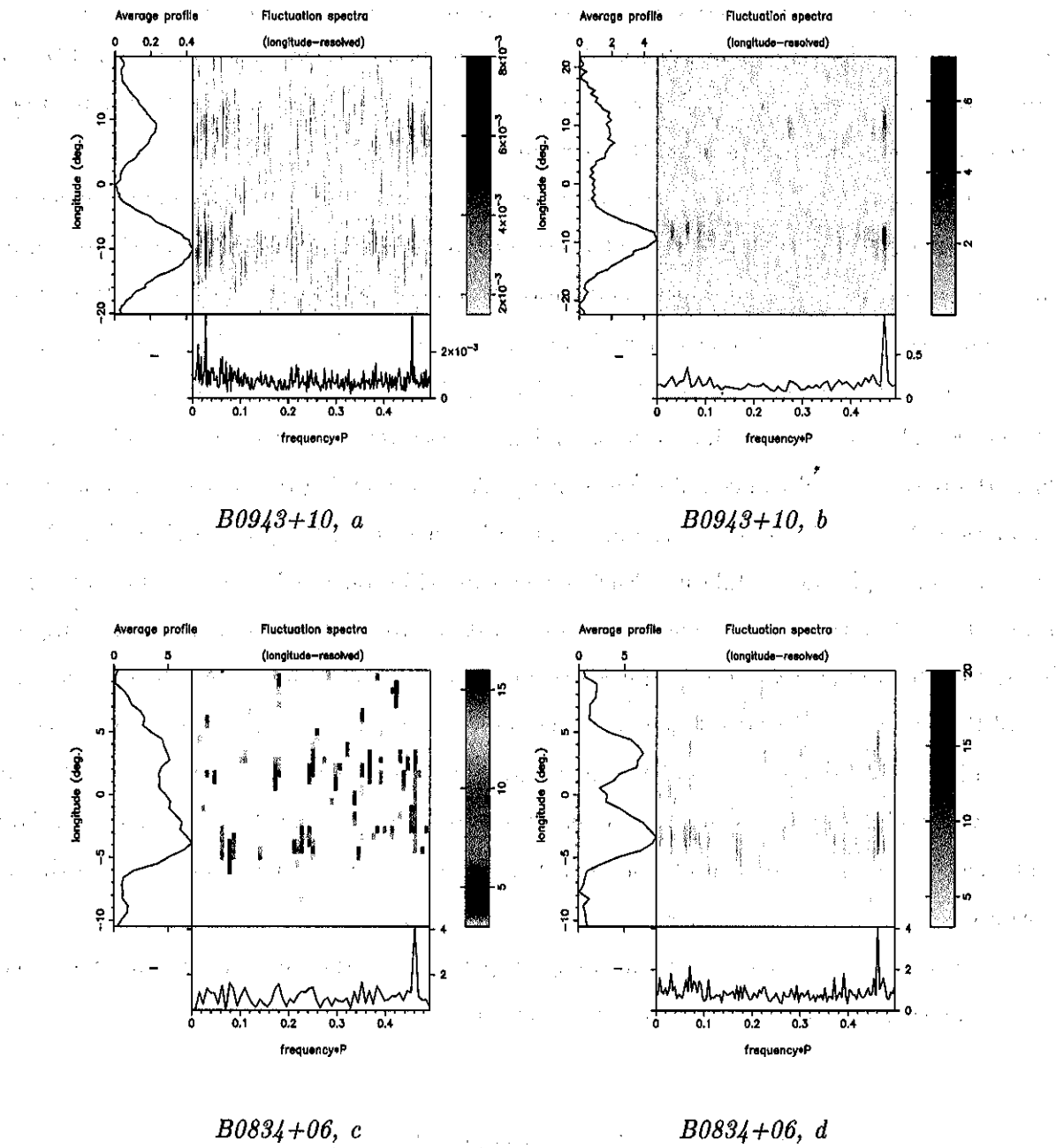

Figure 4.5: Longitude resolved fluctuation spectra (lrf-spectra) of pulsars B0943+10 (a, b) and B0834+06 (c, d) at 35 MHz. Both pulsars display stable fluctuation features in their spectra. At meter wavelengths these features are related to the observed subpulse modulations. *See* the text for more details.

variation is not very unusual, and is observed even at meter wavelengths.

The hrf-spectrum of the pulsar in figure **4.6** displays a strong peak at $0.53\,c/P_1$. From the earlier discussion and the figures **4.2, 4.3,** and **4.4,** it is clear, that the phase modulation feature is aliased and probably represents its true frequency in the hrf-spectrum. If true, this means that the subpulses drift in a direction opposite to the pulsar rotation. The frequency and high-Q nature of the fluctuation matches with the higher radio-frequency results. The raw hrf-spectra, in figure **4.6,** provide the same information about the spectrum, albeit in a different way as described earlier.

Along with the previously known primary modulation feature in the fluctuation spectra at meter wavelengths, one unique feature appears in the decameter spectrum only in one data set. This feature is seen in figure **4.5** clearly at $0.027\,c/P_1$.

B0834+06

This pulsar profile type is classified to be a conal double, and its average profile at decameter wavelengths shows a bridge of emission between the components. The lrf-spectra are displayed in figure **4.5** (c, d), where the spectra were obtained using **128** and **256** pulses respectively. The strong feature close to $0.5\,c/P_1$ appears resolved in the latter spectrum, which suggests its Q-value $\gtrsim 100$. This feature is related to the dramatic alternate-pulse modulation observed in the case of this pulsar. The frequency of the feature in figure 4.5(c) is $0.461\,c/P_1$, which agrees well with results obtained at meter wavelengths.

An hrf-spectrum of this pulsar is shown in figure **4.6.** The true nature of the modulation, *i.e.* amplitude modulation, is apparent from the presence of two strong, near symmetric features around $0.5\,c/P_1$. A raw spectrum for B0834+06 is displayed in figure **4.6.**

B0950+08

This pulsar has the shortest period of all the pulsars in our list, and shows profile bifurcation at decameter wavelengths. Our time resolution appears adequate to slightly resolve the profile components, and study the lrf-spectra under different components and the cross-correlation properties of the components. This pulsar displays a flat, featureless lrf-spectrum, as displayed in figure **4.7.** The peak close to zero frequency arises due to slow variation in the pulsar flux, only a small part of which could be due to scintillations (given that our bandwidth is much larger than the decorrelation bandwidth of scintillations). Intrinsic variability was present as well, on time scales of about **100** pulses ($\sim$ **25** seconds). There are some signs of low level interference in the data. Careful removal of interference has suppressed its effect by a factor of $\geq$ **100** here, otherwise it would give

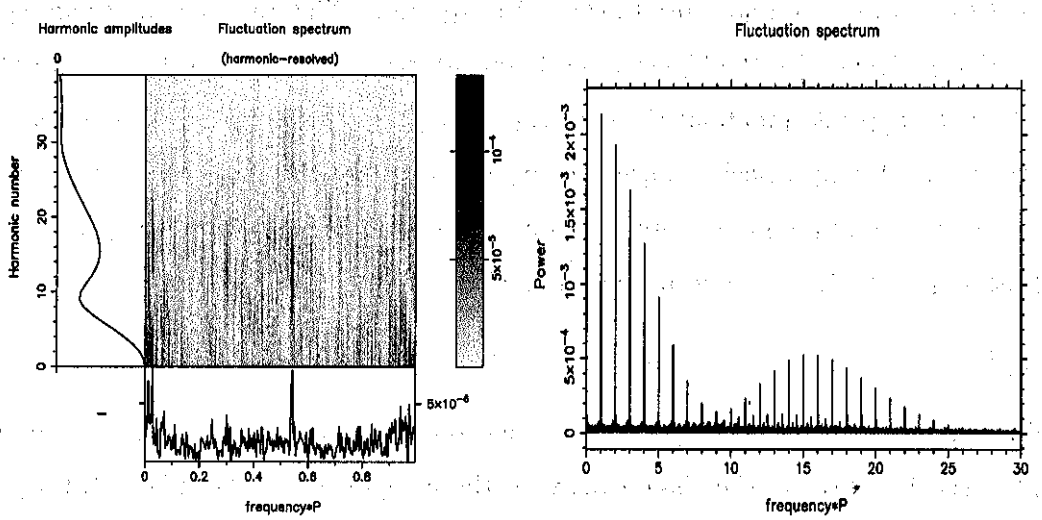

B0943+10 raw *spectrum*

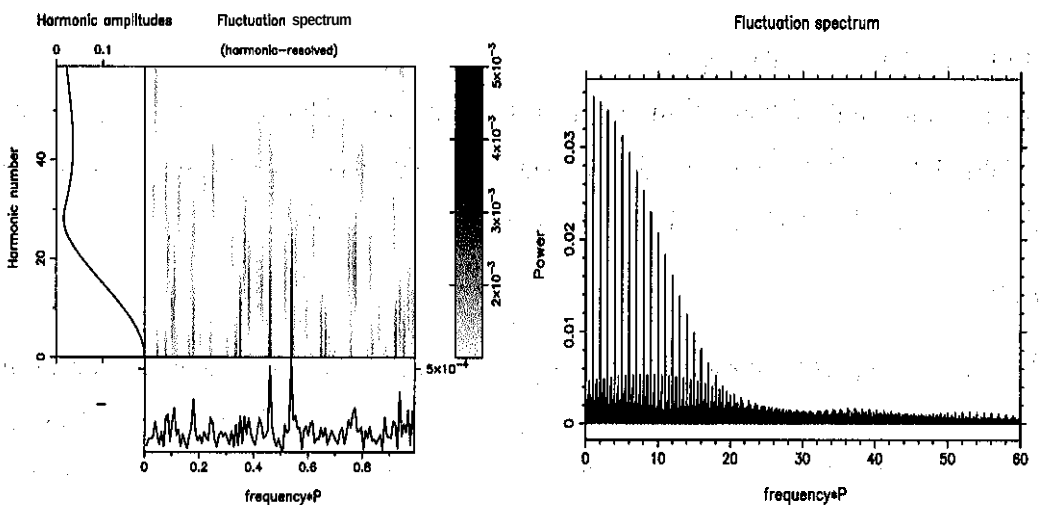

B0834+06 raw spectrum

Figure 4.6: Hrf-spectra of B0943+10 and B0834+06.

rise to some structure in the sum spectrum displayed in the bottom panel of the plot.

B1133+16

The pulsar was detected with a high signal-to-noise ratio in our observations, and shows "double" profile, where the components are completely resolved. The raw spectra obtained, even after some careful interference excision, are found to be contaminated by interference at frequencies ~ 45 **Hz.** The spectrum in figure 4.7 shows two features, and the feature close to $0.1\,c/P_1$ seems believable. We examine it in the hrf-spectrum of the pulsar (figure 4.8), and find it aliased close $0.9\,c/P_1$. We suspect that it is related to amplitude modulation of the two components.

B2016+28

This pulsar is known for its steady subpulse drift observed at meter wavelengths, and the lrf-spectrum in figure 4.7 displays a strong feature close to $0.11\,c/P_1$. The frequency of this feature matches well with that at higher radio frequencies and the hrf-spectrum (figure 4.8) clearly identifies it to be predominantly a phase modulation even at decameter wavelengths.

B1919+21

This pulsar shows a single component at decameter wavelengths. The lrf-spectrum, displayed in figure 4.7, shows a peak at $0.269\,c/P_1$. The other sharp feature in the spectrum falls close to $0.1\,c/P_1$. Both features appear at the same location in the hrf-spectrum, shown in figure 4.8.

B0320+39

The fluctuation behavior of this pulsar was immediately visible even at the average-profile level, with the average profiles made with the successive multiples of the pulse period showing strong variation in their structure. The profile, a "double" at 102 **MHz,** is smeared by the averaging process necessary to detect the weak pulse and hence appears as a single. The lrf-spectrum is shown in figure 4.7, which displays a broad fluctuation feature close to $0.2\,c/P_1$ (see the central panel of the plot). The apparent frequency of the modulation was estimated to be $0.187 \pm 0.014\,c/P_1$, and is most likely to be related to the reported subpulse drift phenomenon at meter wavelengths.

B0628-28

The pulse from this pulsar appears as a single broad peak in our data. The spectrum shows a marginal peak at $0.2\,c/P_1$, but we note that no fluctuation feature was reported in the case of this pulsar previously.

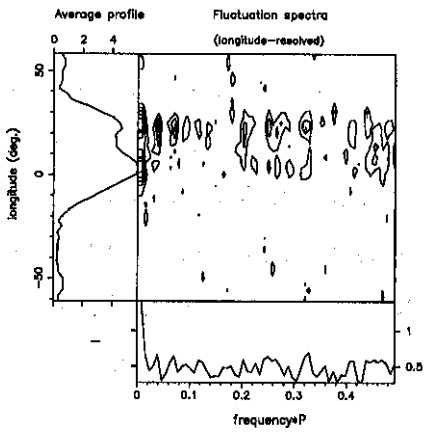

B0950+08, 8th Feb 1999b

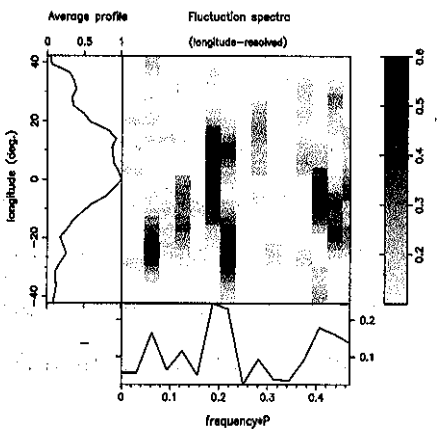

B0628-28 25th Feb 1997

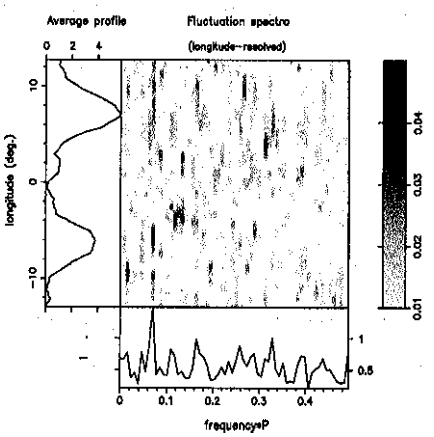

B1133+16, 8th Feb, 1999

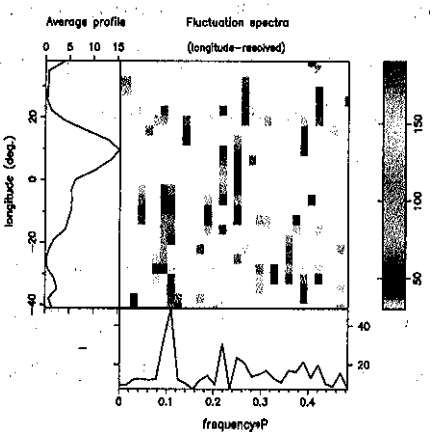

B2016+28 27th June, 1997

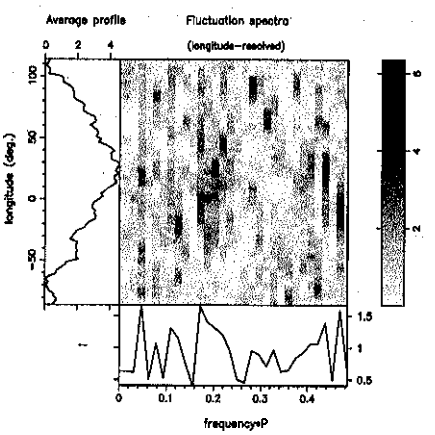

B0320+39, 9th April, 1997

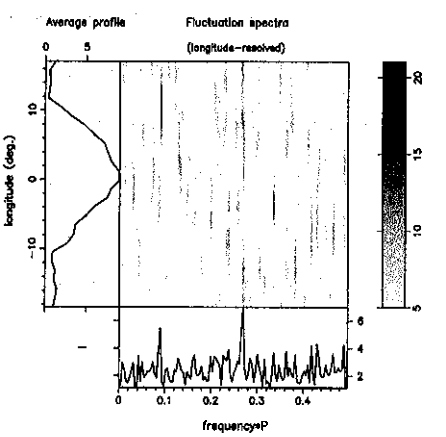

B1919+21 27th June 1997

Figure **4.7:** Lrf-spectra of pulsars at 35 MHz. See the text for details about each pulsar.

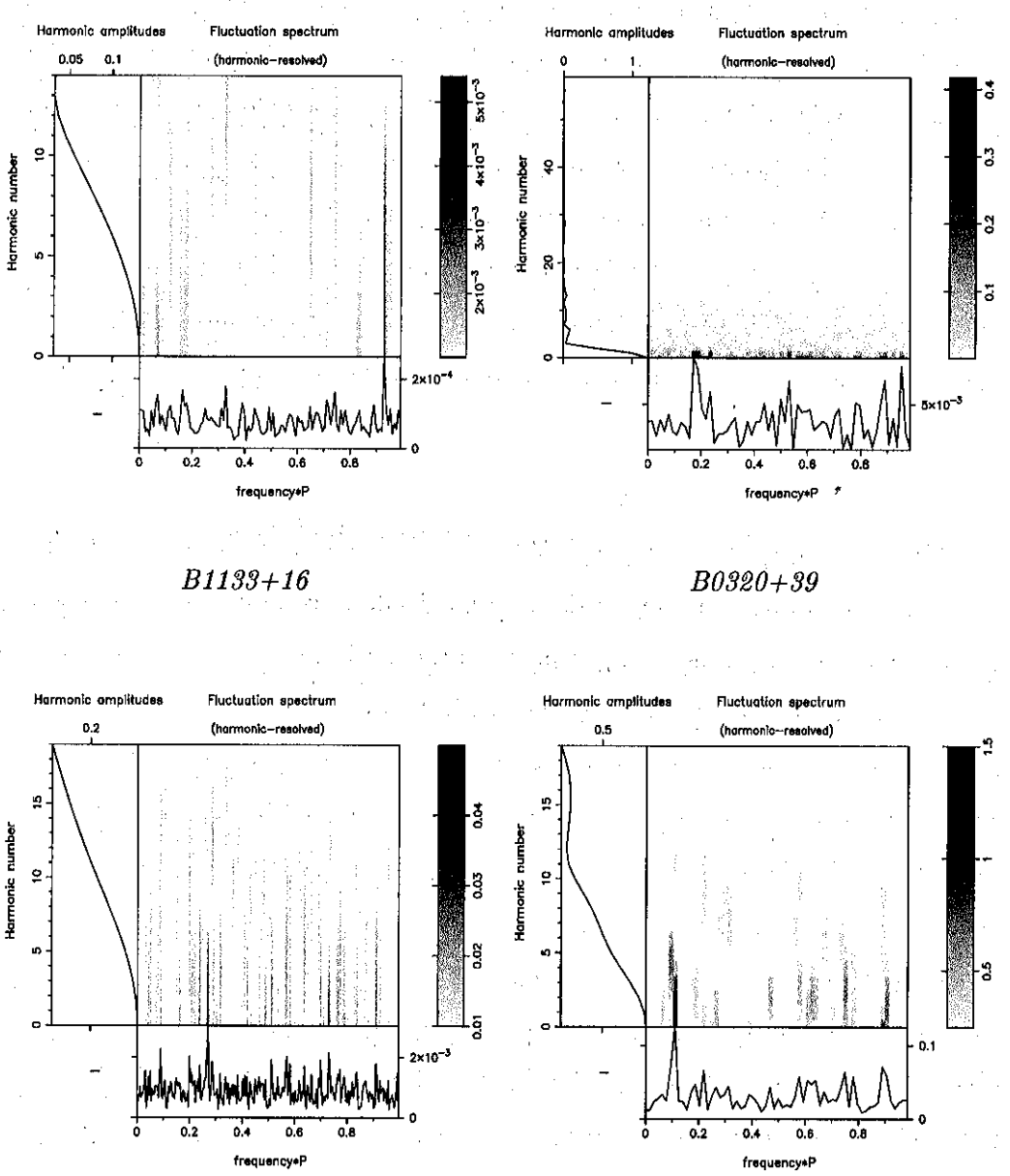

Figure 4.8: Hrf-spectra of some other bright pulsars in our sample.

4.3 Correlation maps

The lrf- and hrf-spectra are best suited to study periodic modulations, and in particular the drift phenomena. But, for some cases, where no apparent drift is observed, and/or where the amplitude modulation may not very periodic, useful information can be sought through suitable time-domain analysis. To investigate a mutual dependence of fluctuations at different longitudes, a cross-correlation analysis of intensity fluctuations at different pulse longitudes is performed (Kardashev et *al.*, 1986). In this section, we detail issues related to cross-correlation maps over the entire pulse region **(2-D)** with a fixed pulse number delay. In a later part of this section, we present the relevant correlation analysis of the data on all pulsars discussed in the previous section.

From a 2-D array of the observed intensities $I(\varphi, \mathrm{k})$, we can compute the the cross-correlation coefficient between intensity fluctuations at different longitudes φ_i and φ_j and pulse delay, μ, according to

$$C_{i,j}(\mu) = \frac{1}{\sigma_i \sigma_j (N - \mu)} \sum_{m=1}^{N-\mu} (I(\varphi_i, m) - \bar{I}(\varphi_i)) \times (I(\varphi_j, m + \mu) - \bar{I}(\varphi_j)) \qquad (4.1)$$

where σ_i designates *rms* variation in intensity at a longitude φ_i computed over N successive pulses. $\bar{I}$ denotes the mean over N pulses, and μ represents the lag in pulse number. An example of such a plot for the pulsar B0834+06 for $\mu = 0$ is shown in figure 4.10.

There are certain points to be noted in figure 4.10. The cross-correlation coefficient peaks diagonally, and the 'components' in the average profile are marked by characteristic square-shaped correlation patterns in the central panel, as marked by A and B in the plot. Any correlated fluctuations between components would produce significant cross-correlation between two points similar to that denoted by C. In general, such maps would show complex patterns when many components are involved. In the case of a systematic linear drift, this would result in parallel diagonal bands of high correlation, separated by a longitude distance of P_2, appearing in the map. The cross-correlation would otherwise drop to zero away from the profile-component longitudes, and the noise is anyway expected to be uncorrelated with itself for any delays beyond the longitude resolution.

B0943+10

The correlation map at zero delay clearly demarcates the two components along the diagonal, and also shows added higher correlation between the components separated by 20° (figure 4.10). The subpulse drift signature in terms of diagonal bands in such maps seen at higher frequencies is not

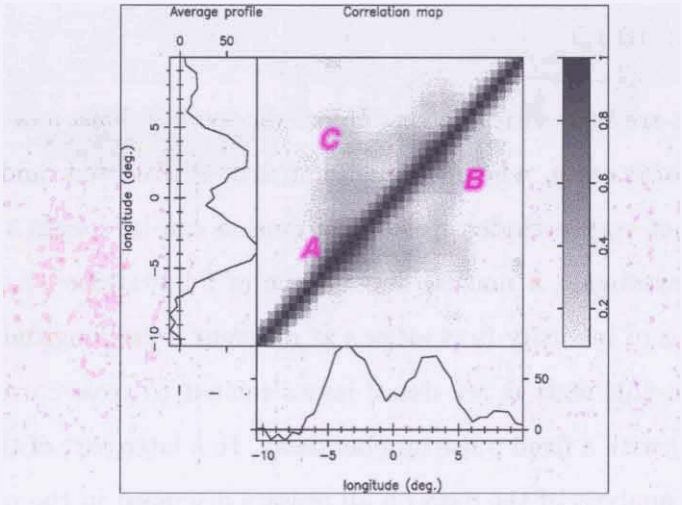

Figure 4.9: Auto-correlation of a B0834+06 pubs sequence with itself on the left, with delay $\mu = 0$, plotted in grey-scale. The diagonal peak is accompanied by some correlation between profile components, related to subpulse fluctuations. In all our plots the pulse sequences denoted by the vertical longitude scale —the left panel profile— are delayed (μ pulse delays).

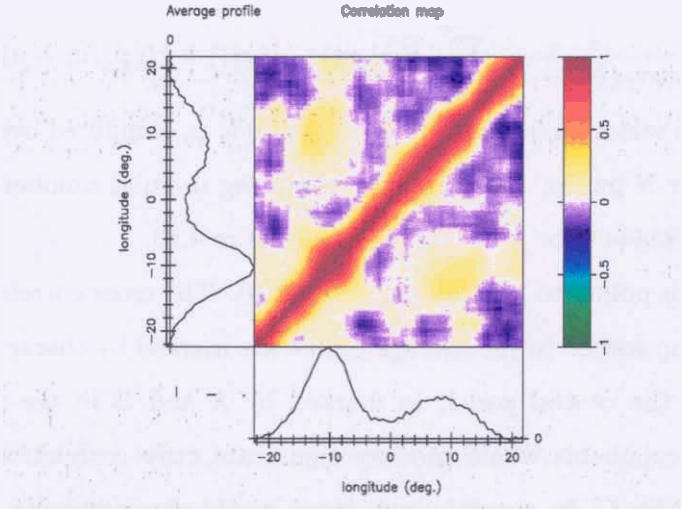

Figure 4.10: Auto-correlation of a pulse sequence for B0943+10. Note the significant correlation between the two components within the same pulse. The distance of such a correlation from the diagonal band is $\sim 20°$, consistent with the component separation.

directly apparent here at decameter wavelengths, due to the effect of more central line of sight (higher β/ρ).

B0834+06

The amplitude fluctuations in the components are clearly seen from the 2-D correlation plots, with pubs delays of $\mu = 1$ and $\mu = 2$ (figure 4.11). The well-known alternate pulse modulation is clearly visible from the comparison of these two maps and the circulation appears to be clearly

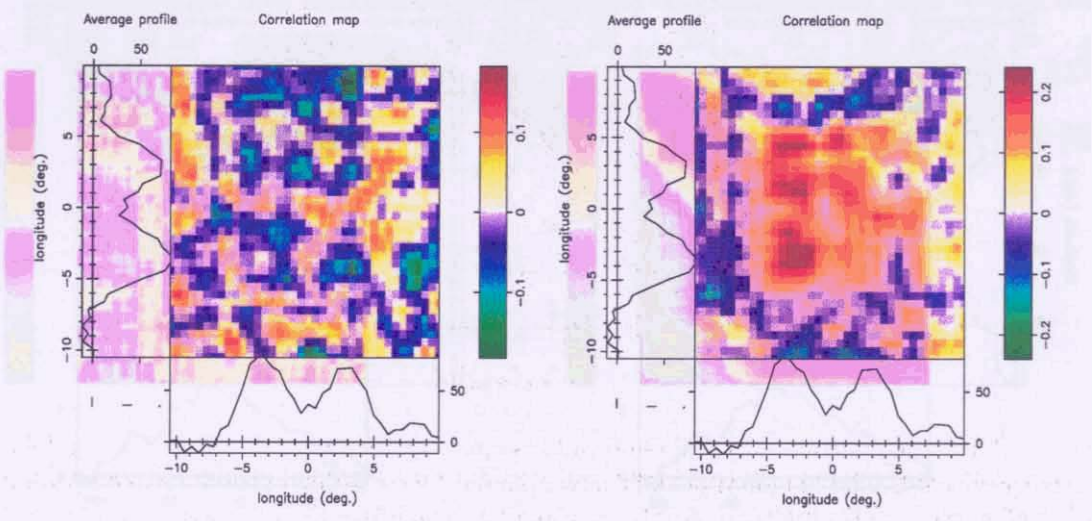

delay $\mu = 1$ *delay* $\mu = 2$

Figure 4.11: Auto-correlation of a B0834+06 pulse sequence with itself with delay $\mu = 1$, plotted as a color scale, the entire pulse is almost anti-amelated after one pulse delay. There is significant correlation for the delay $\mu = 2$ between longitudes. This points to a subpulse "motion" from earlier to later longitudes.

from −ve to +ve longitudes.

B0320+39

The profile in the case of this pulsar is classified to belong to S_d-type in Rankin's scheme. The correlation map for zero delay is shown in figure 4.12. The pulse was further smoothed for detection. This pulsar shows strong fluctuations at decameter wavelengths, which are apparent even in the average profile studies (section 3.1.2).

B1133+16

The two components appear clearly separated in some parts of data, but appear to be bridged in the average profiles from certain other sections. The auto-correlation with delays $\mu = 0$ and $\mu = 1$ is displayed in figure 4.12. The pulse shows significant negative correlation (a coefficient close to -0.4) for a delay $\mu = 2$.

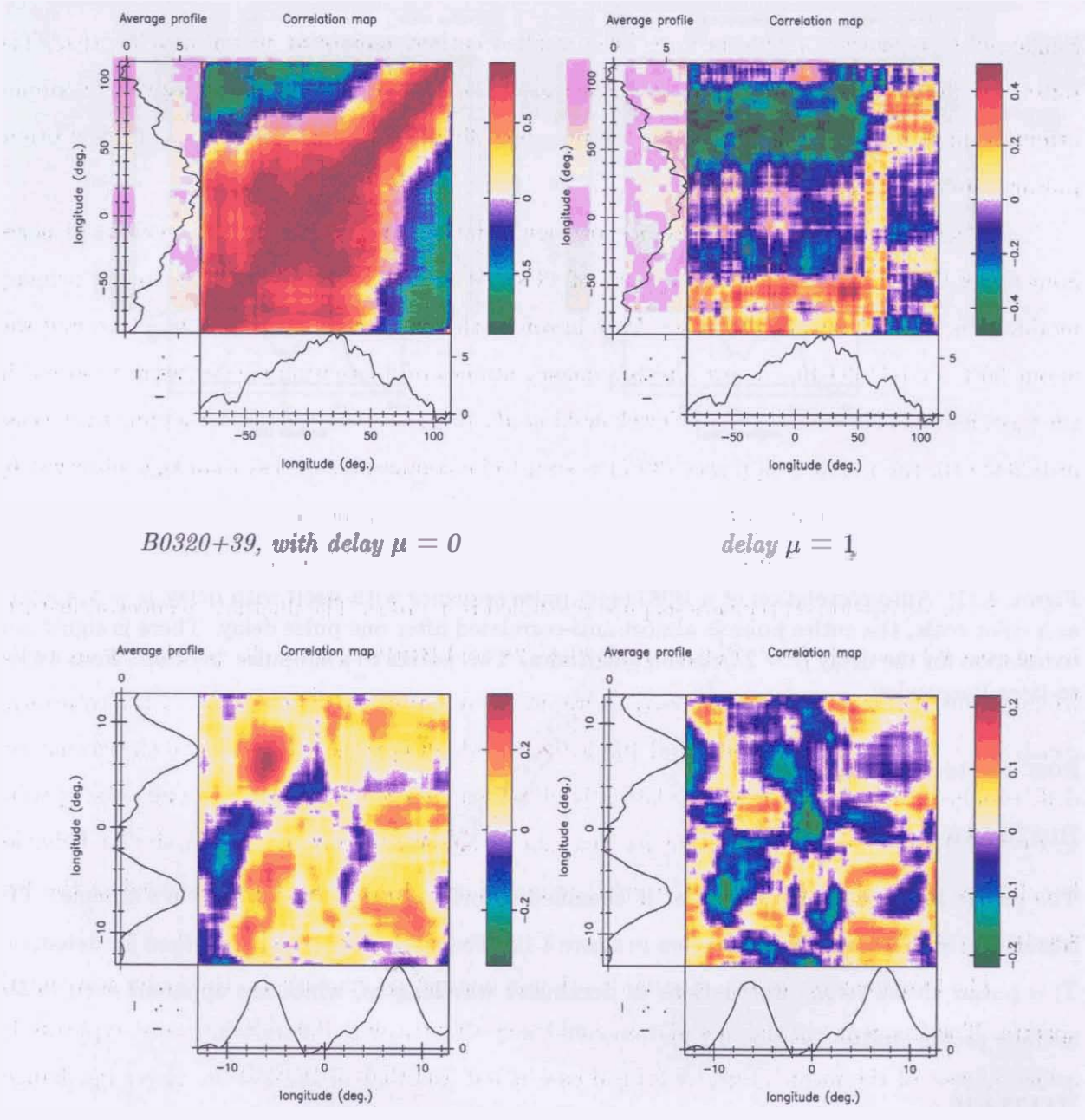

B0320+39, with delay $\mu = 0$ *delay $\mu = 1$*

B1133+16, with delay $\mu = 1$ *delay $\mu = 2$*

Figure 4.12: Top: Auto-correlation of a B0320+39 pulse sequence with itself with different delays. The correlation at $\mu = 0$ shows the possibility of another component in the wide pulse at its edge. Almost the entire pulse displays null correlation after one pulse delay, though there is significant correlation between the edge of the pulse and its peak. **Bottom:** There is considerable fluctuation around the mean power of B1133+16. The correlation maps with delays of 1 and 2 pulses are presented. The significant asymmetry in the case of $\mu = 1$ suggests the circulation from $-ve$ to $+ve$ longitudes.

4.4 Discussion and comparison with earlier work

Single-pulse sequences of pulsars have been studied earlier, mostly at meter wavelengths. The pulsars with drifting subpulse emission, such as B0943+10, B0809+74 *etc*, received maximum attention in this regard. In this chapter we presented fluctuation-spectral analysis of a few bright pulsars observed at 35 MHz.

It is a general result that pulsars show significant fluctuation even at these low frequencies. Sometimes the entire power in a sequence of B0834+06 was observed to belong to the primary modulation, while it dropped to about 50% in some other sequences for the same pulsar, and was about 30% for B1133+16. A few multi-frequency studies of fluctuation spectra were reported in the past, and we refer the reader to Nowakowski *et al.*, 1982, and the references therein. In the case of B0943+10, the fluctuation power (30%) is seen to be comparable or less than that observed by Deshpande and Rankin at meter wavelengths. As we discuss in the next chapter, the fluctuation properties for a pulsar in the same sequence seem to vary considerably at 35 MHz.

Some discussion on the various pulsars studied is in order. The fluctuation spectral features in the case of known 'drifters', B0943+10, B2016+28, and B1919+21, are sharp. The feature in the lrf-spectrum of B0943+10 remains partly unresolved even after using 512 pulses in the transform, consistent with the spectra at 430 and 100 MHz. The high Q-value of the feature shows that the drift process giving rise to the modulation is highly stable even at 35 MHz, though the Q-value was certainly lower in our data compared to that in meter-wavelength data. A similar behavior is exhibited by B1919+21, where the primary modulation feature is almost resolved in the hrf-spectrum with 256 pulses.

The frequency of the primary modulation in our spectra match with the meter-wavelength spectra. The frequency of the modulation could vary slightly over different data sets, typically by a few percent of the mean value. A typical case noted was that of B0943+10. Here, P_3 changes by $\sim$ 1% in our various data sets, though the Q-value remains more than 100 in each sequence. Such a variation in P_3 was noted even by paper-I. Similar trends were seen for B0834+06, where more than one data set were studied at 35 MHz. The central frequency of the modulation remains unchanged with the radio frequency of observation, however, *irrespective* of whether the feature is broad or narrow. This is to say, that the average frequency is unchanged even in the cases where the modulation is erratic, and which produce broad features in the spectra.

A remarkable observation was noted in the case of B0320+39. The modulation appears to be so strong in the case of this pulsar, that it was apparent from the average profiles made

at multiples of the true period of the pulsar (as noted in chapter 3). The fluctuation does not appear so prominently in the lrf-spectrum. The pulsar B1133+16 displays a broad fluctuation at low fluctuation frequencies, and was studied for correlation maps with diierent delay settings. B0950+08 shows a featureless spectrum, and this is consistent with its higher frequency behavior, though the data seems to contain some low level interference. Pulsar B0628–28 has the highest DM of 35 for a pulsar in our sample. Its pulse appears broad. The lrf-spectrum shows a weak feature (at $\sim 0.2\, c/P_1$) which was probably not noticed in any of the meter-wavelength studies.

4.5 Summary

In this chapter, we discussed the conventional tools to study the various types of single-pulse fluctuation phenomena, which include the fluctuation spectra and correlation analysis. We studied eight bright pulsars in our observed sample for their single-pulse properties.

A very powerful and conventional tool, 'longitude resolved fluctuation spectra' (lrf-spectra; Backer, 1973), brings out any systematic of single-pulse fluctuations as a function of time (pulse number) and pulse longitude much more clearly than possible in the time domain. However, such spectra have a serious drawback of aliasing. Such an aliasing hinders determination of the exact frequency of a spectral feature and any possible harmonic relationship between various features.

To address the issue of aliasing in spectra, we follow the approach taken by Deshpande & Rankin (1999: DRa, 2001:paper-I). We Fourier transform the entire continuous pulse sequence, which can be reconstructed (from the "gated" version) by using the available samples on within the pulse window, and filling the unsampled longitude (off-pulse) region with zeros. We choose to present the raw fluctuation spectrum in another manner, where we stack the successive sections of the spectrum of width $(1/P_1)$. We refer to this spectral representation an "harmonic-resolved fluctuation spectrum", or an HRF-spectrum.

Such an hrf-spectrum does not have the same limitations of sampling as does an lrf-spectrum. An hrf-spectrum can further distinguish between the two types of pulse modulations encountered, *viz.* amplitude- and phase-modulations. However, an hrf-spectrum does not resolve the issue of aliasing entirely on its own. One has to invoke further constraints to understand any possible aliasing of features. Various issues regarding lrf- and hrf-spectra were discussed in sections 4.2.1 and 4.2.2.

We have presented fluctuation-spectral analyses of 8 bright pulsars in this chapter, and discussed the individual cases. It is found, in general, that pulsars show significant fluctuation even at these low frequencies. Fluctuation power (as a function of the total) varies from pulsar to pulsar, and in some pulse sequences the entire fluctuation power was observed to belong to the associated primary modulation. The fluctuation spectral features in the case of known 'drifters', B0943+10, B2016+28, and B1919+21, are sharp. The feature in the lrf-spectrum of B0943+10 remains partly unresolved even after using 512 pulses in the transform, consistent with the spectra at 430 and 100 MHz. The high Q-value of the feature shows that the drift process giving rise to modulation is remarkably stable even at 35 MHz, though the Q-value was certainly less in our data compared to that in meter-wavelength data.

The frequencies of the primary modulation in our spectra show a reasonable match with those observed in the meter-wavelength fluctuation spectra. The frequency of the modulation could vary slightly over different data sets, typically by a few percent of the mean value. The average frequency of the modulation remains unchanged with frequency, however, irrespective of whether the feature is broad or narrow. This is to say, that the frequency is unchanged even in the cases where the modulation appears to be erratic and has thus produced broad features in the spectra.

The Irf- and hrf-spectra are best suited to study periodic modulations, and in particular the drifting-subpulse phenomenon. But, for some cases, where no apparent drift is observed, and/or where the amplitude modulation may not very periodic, useful information can be sought through suitable time-domain analysis. To investigate a mutual correspondence between the fluctuations at different longitudes, a cross-correlation analysis of intensity fluctuations at different pulse longitudes was performed. In section 4.3, we detailed issues related to cross-correlation maps over the entire pulse region **(2-D)** with a fixed pulse-number delay. We have presented the relevant correlation analysis of the data on all pulsars discussed in the previous section. An asymmetry in the correlation maps for one- and two-pulse delays in the case of B0834+06 and B1133+16 offers a possible solution to the drift direction in the case of these two pulsars.